Decompression-Induced Diamond Formation from Graphite Sheared under Pressure

Jiajun Dong,[1] Zhen Yao,[1] Mingguang Yao,[1,*] Rui Li,[2] Kuo Hu,[1] Luyao Zhu,[1] Yan Wang,[1] Huanhuan Sun,[1] Bertil Sundqvist,[3] Ke Yang,[4] and Bingbing Liu[1,†]

[1]*State Key Laboratory of Superhard Materials, College of Physics, Jilin University, Changchun 130012, China*
[2]*Institute of Materials Science and Engineering, Changchun University of Science and Technology, Changchun 130022, China*
[3]*Department of Physics, Umeå University, SE-90187 Umeå, Sweden*
[4]*Shanghai Synchrotron Radiation Facilities, Shanghai Institute of Applied Physics, Chinese Academy of Sciences, Shanghai 201204, China*

(Received 3 October 2019; accepted 9 January 2020; published 10 February 2020)

Graphite is known to transform into diamond under dynamic compression or under combined high pressure and high temperature, either by a concerted mechanism or by a nucleation mechanism. However, these mechanisms fail to explain the recently reported discovery of diamond formation during ambient temperature compression combined with shear stress. Here we report a new transition pathway for graphite to diamond under compression combined with shear, based on results from both theoretical simulations and advanced experiments. In contrast to the known model for thermally activated diamond formation under pressure, the shear-induced diamond formation takes place during the decompression process via structural transitions. At a high pressure with large shear, graphite transforms into ultrastrong sp^3 phases whose structures depend on the degree of shear stress. These metastable sp^3 phases transform into either diamond or graphite upon decompression. Our results explain several recent experimental observations of low-temperature diamond formation. They also emphasize the importance of shear stress for diamond formation, providing new insight into the graphite-diamond transformation mechanism.

DOI: 10.1103/PhysRevLett.124.065701

Being the hardest material in nature, diamond has been widely used in various applications [1–3]. Diamond can be obtained as a natural mineral, but it can also be synthesized on an industrial scale [4,5]. Catalyst-free synthesis of diamond through the compression of graphite at a high temperature and by shock compression has attracted intense research interest for several decades [6–11]. The mechanism for the transformation of graphite into diamond under pressure has been discussed in terms of either a concerted mechanism or a nucleation mechanism [12–16]. In these mechanisms, graphite may transform directly into diamond via the appropriate sliding and buckling of graphitic planes upon compression or shock, as has been reported in experiments [11]. Sliding of graphite planes changes the symmetry of the graphite structure and provides transformation pathways from rhombohedral graphite to cubic diamond and from orthorhombic graphite to hexagonal diamond [13,16]. Note that, for activating the sliding and buckling of graphite planes and making any diamond structure formed quenchable to ambient, a high temperature at high pressure is necessary [16]. This is normally associated with shock compression but must be supplied externally in static experiments. The synthesis of diamond by compression at room temperature or a low temperature is, in contrast, rare and not well understood. It is, therefore, both interesting and surprising that several recent publications report observations of diamond together with other carbon phases in carbon materials such as graphite, fullerenes, or graphene, etc., released after room-temperature compression under nonhydrostatic pressure conditions with strong shear stress [17–20]. The formation of diamond under such conditions of compression seems to be anomalous and cannot be explained by the transition mechanisms proposed earlier. For example, Gao *et al.* recently reported that graphite transforms into sp^3 carbon phases (considered as hexagonal diamond) at a low pressure if a large plastic shear is added, while they observed nanocrystalline cubic diamond instead of hexagonal diamond in the sample after decompression [18]. Shiell *et al.* found that glassy carbon transformed into transparent sp^3-rich structures at 100 GPa and the relatively low temperature of 400 °C. It is strange that upon decompression to ambient pressure the central part of the sample, which is transparent at a high pressure, transforms back to a graphitic phase, while the area at the chamber edge is transformed into transparent diamond nanocrystallites, likely in a hexagonal structure [21,22]. It is suggested that a large shear stress created at the chamber edge plays an important role for the formation of diamond.

It seems that diamond formation in these experiments deviates from the known diamond formation mechanisms [13,16], which operate during the decompression process under such nonhydrostatic pressure conditions. However, the underlying microscopic mechanism is still unclear.

To explain these puzzling observations, we here report a new transition pathway for graphite into diamond under compression with an added shear, based on theoretical simulations and well-controlled experiments. This transition pathway leads to the formation of diamond during the decompression process via structural transitions and is able to explain the puzzles in the previous literature.

In our calculations, a shear model is designed to generate shear stress and simulate the shear-induced transformations in graphite. The calculations are based on the density functional theory (DFT) [23,24] implemented with the Vienna *ab initio* simulation package (VASP) [25–27] (for details of the simulation, see Supplemental Material [28]). In our simulation, hexagonal graphite ($3 \times 3 \times 2$ hexagonal supercell) is hydrostatically compressed up to 20 GPa, at which no interlayer bonding occurs in graphite [Fig. 1(a)]. Then, based on the optimized high-pressure structure, a series of shear operations are applied via different sliding angles θ and ω [Figs. 1(b) and 1(c)]. After this shear operation, each carbon atom exhibits a relative displacement vector of $[\boldsymbol{d}\sin\boldsymbol{\theta}\cos\boldsymbol{\omega}, \boldsymbol{d}\sin\boldsymbol{\theta}\sin\boldsymbol{\omega}, \boldsymbol{d}\cos\boldsymbol{\theta} - \boldsymbol{d}]$, where d is the interlayer spacing of graphite at 20 GPa. These shear operations lead to sliding and buckling of graphite planes and result in various sp^3 carbon structures via some interlayer bond formations. The new structures include few layered diamond and sp^3-carbon structures with symmetry groups P-1 or $C2/m$ (Table I), but their lattice parameters and atomic coordinates differ depending on the shear operations applied. Similar layered diamond structures have been proposed as an intermediate phase for the transition from graphite to diamond during shock compression, where they form by buckling of the basal planes in ultrafast *ab initio* molecular dynamics simulations [24]. To our surprise, these high-pressure structures are not stable and transform into the graphite or diamond structures when pressure and stress are released, as shown in Table I.

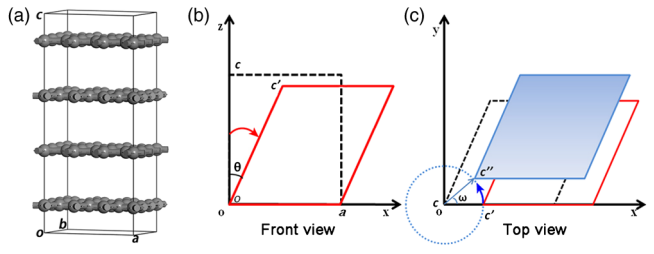

FIG. 1. (a) Optimized structure of hexagonal graphite hydrostatically compressed to 20 GPa. The lattice constants oa (ob) and oc are 7.3 and 11.3 Å, respectively. The interlayer spacing is 2.82 Å. (b),(c) Schematic illustration for the calculations on graphite under shear stress. During the simulation, the lattice is first sheared by rotating the oc by an angle θ toward the x axis (b). After this, a rotation perpendicular to the z axis by an angle ω is applied for further shear operation. The blue rhomb in (c) represents the position of the top graphene plane of the graphite cell after the shear operation.

Both the layered diamond structures and the sp^3 carbon phases could transform into the diamond structure via structural transitions upon decompression. Figure 2 shows two alternative paths for the transformation from graphite to interlayer-bonded carbon phases upon compression with shear stress and then to diamond upon decompression. Figures 2(a)–2(d) show the case of a layered diamond structure ($C2/m$) under the shear operation $\theta = 44°$ and $\omega = 90°$ at 20 GPa, while Figs. 2(e)–2(h) show the case of an sp^3 carbon structure with P-1 symmetry with the shear operation $\theta = 45°$ and $\omega = 0°$. Thus, by applying different shear stresses to compressed graphite, metastable sp^3 phases with various structures could be formed, and these then transformed into either diamond or graphite via phase transitions upon decompression. These results clearly show that diamond formation may occur via structural transitions during the decompression process from graphite submitted to shear stress at a high pressure. Furthermore, our simulations also demonstrate that the shear stress plays a vital role for interlayer bonding in graphite under a high pressure.

To verify our theoretical predictions, we designed high-pressure experiments on nanocrystalline graphite

TABLE I. The shear operations and transformations of graphite at 20 GPa.

Θ	ω	Interlayer bond	Released
40	0	No	Graphite
40	30	Layered diamond ($C2/m$)	Cubic-diamond
40	60	No	Graphite
40	90	Layered diamond ($C2/m$)	Cubic-diamond
41	0	No	Graphite
41	30	Fully sp^3 ($C2/m$)	Cubic-diamond
41	60	No	Graphite
41	90	Fully sp^3 ($C2/m$)	Cubic-diamond
42	0	No	Graphite
42	30	Fully sp^3 ($C2/m$)	Cubic-diamond
42	60	No	Graphite
42	90	Fully sp^3 ($C2/m$)	Cubic-diamond
43	0	No	Graphite
43	30	Fully sp^3 ($C2/m$)	Cubic-diamond
43	60	No	Graphite
43	90	Fully sp^3 ($C2/m$)	Cubic-diamond
44	0	No	Graphite
44	30	Layered diamond ($C2/m$)	Cubic-diamond
44	60	Fully sp^3 (P-1)	Cubic-diamond
44	90	Layered diamond ($C2/m$)	Cubic-diamond
45	0	Fully sp^3 (P-1)	Cubic-diamond
45	30	Layered diamond ($C2/m$)	Graphite
45	60	Layered diamond (P-1)	Cubic-diamond
45	90	Layered diamond ($C2/m$)	Graphite
50	0	Layered diamond (P-1)	Cubic-diamond
50	30	Layered diamond ($C2/m$)	Graphite
50	60	Fully sp^3 (P-1)	Cubic-diamond
50	90	Layered diamond ($C2/m$)	Graphite

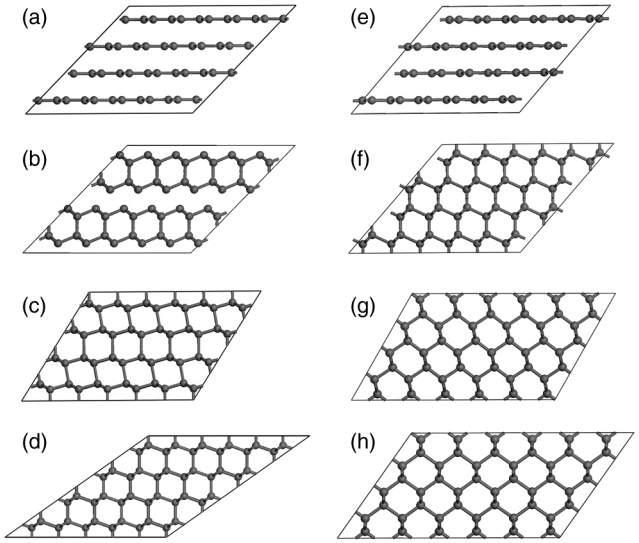

FIG. 2. Two examples [(a)–(d) and (e)–(h)] of the transformation pathway for hexagonal graphite to diamond under 20 GPa with different shear stresses. (a),(b) The formation of a layered diamond structure ($C2/m$) under the shear operation $\theta = 44°$, $\omega = 90°$ at 20 GPa. (c) Snapshot of layered diamond during decompression. The lattice distorts and diamond layers bond into a fully sp^3-bonded structure. (d) Transformation into cubic diamond upon decompression to atmospheric pressure. (e),(f) The formation of an sp^3 carbon structure with P-1 symmetry group under the shear operation $\theta = 45°$, $\omega = 0°$. (g) Snapshot of the fully sp^3-bonded structure during decompression. (h) Transformation into cubic diamond when pressure is released.

microspheres (NG spheres) to which we applied shear stress. The shear stress is generated by introducing uniaxial stress on the compressed graphite microsphere by direct contact with the two diamond anvils during compression [33–35]. Two NG spheres with diameters of about 35 and 15 μm, called the L and S sphere, respectively, are loaded into the sample chamber with liquid argon as the pressure medium (for experimental details, see Supplemental Material and Fig. S1 [28]). During the experiments, NG spheres with different sizes would make contact with the two diamond anvils at different pressures. The L sphere will be directly compressed between the diamond anvils above around 10 GPa and a large uniaxial stress will be generated, while the smaller S sphere will never make contact with more than one anvil and, thus, acts as a control sample always kept under quasihydrostatic conditions. We can quantitatively determine the uniaxial stress by estimating the pressure above the indentation point (the center of the sphere, at the upper anvil's culet) from the high-frequency edge of the diamond Raman line [36]. In these experiments, we observed that the indentation pressures (P_{ind}) between the L sphere and the anvil became much higher than the chamber pressure (P_{cham}) [Fig. 3(a)]. The pressure difference ($\Delta P = P_{\mathrm{ind}} - P_{\mathrm{cham}}$) increases with increasing P_{cham} and reaches 51 GPa at the chamber pressure $P_{\mathrm{cham}} = 52$ GPa, while the circular outline of the sphere is still preserved. This suggests that the transformed sphere has an extremely high strength, being able to sustain such a large stress difference. In contrast, the S sphere never shows any obvious indentation pressure relative to the anvils during the whole compression cycle. The pressure difference on the L sphere can be used to evaluate its strength under pressure according to the previous literature [34,37,38], using the following equations:

$$\tau = 1.5 \times (P_{\mathrm{ind}} - P_{\mathrm{cham}}), \tag{1}$$

$$Y = 2 \times \tau. \tag{2}$$

Here τ is the maximum shear stress and Y is the yield strength. The yield strength of the L sphere is found to be about 153 GPa at $P_{\mathrm{cham}} = 52$ GPa, which is even higher than that of the (100) diamond plane at ambient conditions (yield strength $\sim 130 - 140$ GPa) [39] and close to that of nanodiamond [37]. To improve our understanding, we also carried out finite element simulations which showed the shear stress distribution in the L sphere under uniaxial compression [Fig. 3(b); for details, see Supplemental Material [28]]. The stress is concentrated near the contact point and decreases to the chamber pressure along the upper surface, which generates an extremely strong shear stress field in the L sphere.

The significant uniaxial stress difference between the L and S spheres also causes remarkable differences in their Raman spectra upon compression. Figures 3(c) and 3(d) show selected Raman spectra measured at the centers of the two spheres upon compression. We can see that the evolutions of the Raman spectra for the spheres are similar below 10 GPa but become different at higher pressure. The G band of the L sphere shifts up and broadens with increasing pressure up to 24 GPa and transforms into a broad and asymmetric band at higher pressure. Note that at above 24 GPa the frequency of the G band keeps almost constant and even shows a slight downshift [Fig. 3(e)]. It has been suggested that a G-band downshift and a transformation into one broad and asymmetric band is a strong indication for interlayer bonding in carbon materials [34,40,41]. Note that the presence of a large uniaxial stress is responsible for this G-band transition, because for the S sphere, which suffers no uniaxial stress upon compression, there is a monotonic upshift in G-band frequency without any indication of a bonding change [42]. We thus conclude that a significant interlayer bonding is triggered in the L sphere at a shear stress around 20–30 GPa, caused by the uniaxial compression (Fig. S2 [28]).

X-ray diffraction measurements (Fig. S3 [28]) further show that, at a pressure of 46 GPa with large uniaxial stress, the large NG sphere exhibits a broad peak in the range of 2.9–3.3 $\mathrm{Å}^{-1}$ while the characteristic (002) peak of graphite

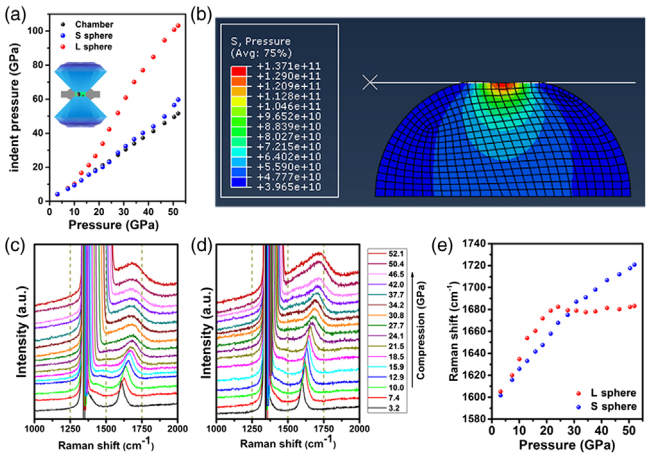

FIG. 3. (a) Pressure at the indenting point of the two NG spheres, measured from the high-frequency edge of the diamond Raman line, as a function of the chamber pressure. The inset shows a schematic illustration of the uniaxial compression experiment. (b) Finite element simulation of the shear distribution in the L sphere under uniaxial compression at a confining pressure of 50 GPa. Raman spectra of (c) the L sphere and (d) the S sphere recorded at selected pressures upon compression. A 514.5 nm laser was used for excitation. (e) The corresponding pressure dependence of the G-band frequencies for the two NG spheres.

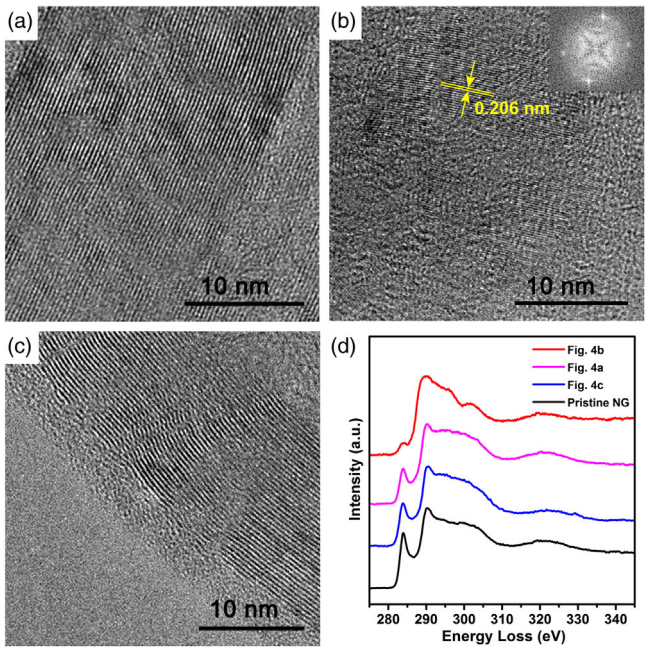

FIG. 4. HRTEM images of the decompressed L sphere, showing the areas containing graphite nanocrystals (a) and diamond nanograins (b). The inset in (b) gives the corresponding diffraction pattern; the angle between the reflexes is about 70°, which is consistent with that between the (111) planes of cubic diamond. (c) HRTEM image of the recovered S sphere showing only nanocrystalline graphite. (d) EELS spectra of decompressed NG spheres measured from the areas indicated in (a)–(c) and a pristine NG sphere.

disappears. In contrast, a detectable (002) peak is preserved in the S sphere (without large uniaxial stress) at 46 GPa, suggesting that the S sphere mainly keeps its graphite structure. Note that the broad diffraction peak in the range of 2.9–3.3Å^{-1} from the L sphere agrees with the main diffraction peaks of one or several of the shear-induced sp^3 carbon structures predicted from our simulations of sheared compressed graphite (Fig. S3 [28]). Based on the MD simulation, graphite under pressure with different degrees of shear stress may transform into sp^3 carbon phases with different structures. Thus, most likely the high-pressure phase(s) of the L sphere under uniaxial compression includes one or several predicted structure(s) from our simulations due to the nonuniform shear stress distribution in the sphere. According to both Raman spectra and x-ray diffraction patterns, the L sphere transforms into ultrastrong, sp^3-rich carbon phases under pressure in the presence of large uniaxial stress.

Raman and TEM measurements were subsequently made on the decompressed samples to see whether these high-pressure phases are quenchable to ambient or not. Raman spectra of the quenched spheres (Fig. S4 [28]) show significant broadening and an increase of D-band intensity for the released L sphere, indicating an irreversible transformation in the released sample [18]. HRTEM images of the decompressed L sphere [Fig. 4] show that, besides the graphite nanograins, some diamond nanograins can be found. Electron energy loss spectroscopy (EELS) [Fig. 4(d)] further shows an obvious reduction of the $\pi*$ peak which confirms the formation of diamond in the L sphere after large uniaxial stress [17,20,43]. In contrast, no diamond can be found in the recovered S sphere. These results agree well with our simulations, which showed that the high-pressure sp^3 carbon phases formed in sheared, compressed graphite could transform into diamond and graphite during decompression. For comparison, an experiment at a higher (quasi)hydrostatic pressure has been performed on a small piece of a NG sample to further explore the transition. Careful TEM observations show that after (quasi)hydrostatic compression of 108 GPa the released sample still preserves its graphitic structure without any diamond formation (Fig. S5 [28]). Therefore, the shear stress induced by our uniaxial compression plays a key role for the graphite-to-diamond transformation in the L sphere following the new transition pathway in our experiments.

In our experiments, an extremely strong shear stress resulting from the large pressure difference between the chamber pressure and the uniaxial stress applied between the two anvils could drive a lattice distortion in the nanocrystalline graphite in the NG sphere, promoting the formation of ultrastrong, sp^3-rich carbon phases. This is also demonstrated by our finite element simulation [Fig. 3(c)]. A similar transformation might also explain the

recent observation of multiple unidentified *in situ* x-ray diffraction rings in the range of 2.73–3.31 $Å^{-1}$ in a rotational diamond anvil cell [18]. These lines might originate from the formation of metastable sp^3 carbon phases as found in our simulations under pressure with shear stress. Moreover, upon decompression these metastable sp^3 phases transform into diamond or graphite, also in agreement with our simulations. These observations may explain earlier reports of mixed phases of nanocrystalline diamond and fragmented graphite in quenched samples after the application of large shear stress [17–18,20–22]. Similarly, our proposed transition pathway may also be used to understand the quenchable diamond structure found in glassy carbon recovered from high pressure and why quenched diamond was found only at the chamber edge, where shear stress is large (compressing glassy carbon to above 45 GPa first leads to graphization) [21,22,44]. Under nonhydrostatic pressure conditions with relatively small shear stress, graphite transforms into high-pressure phase(s) with broad diffraction peaks in the range of 2.70–3.35 $Å^{-1}$ at 65 GPa and transforms back to graphite structure upon decompression, undergoing a reversible phase transition [45]. Our two-step transition pathway from graphite to diamond under compression combined with a strong shear may thus explain several puzzling results in earlier experiments, including the detailed positional distribution of mixed phases of graphitic carbons and nanodiamond grains observed in released samples submitted to different shear stress distributions under a high pressure.

In summary, a novel transformation pathway from graphite to diamond induced by shear stress at room temperature has been demonstrated. With the application of shear stress, compressed graphite first transforms into metastable sp^3 carbon phases under pressure and then transforms into diamond or graphite upon decompression. Our experiments confirmed that, when compressed graphite was submitted to large shear stress by uniaxial compression at a high pressure, ultrastrong, sp^3-rich carbon phases (yield strength could reach 150 GPa at a confining pressure of 52 GPa) were formed. The experimental observations of diamond and graphite in the decompressed samples further support our proposed transformation pathway. Our result emphasizes the importance of shear stress effects on the transformation of graphite to diamond at room temperature and provides new microscopic mechanisms for the graphite-to-diamond transition.

This work was supported financially by the National Key R&D Program of China (No. 2018YFA0305900 and No. 2018YFA0703404), the National Natural Science Foundation of China (51822204, 51320105007, and 11634004), the Program for Changjiang Scholars and Innovative Research Team in University (IRT1132), the Program for JLU Science and Technology Innovative Research Team (No. 2017TD-01), and Graduate Interdisciplinary Research Fund of Jilin University (No. 10183201833).

*yaomg@jlu.edu.cn
†liubb@jlu.edu.cn

[1] T. Irifune, A. Kurio, S. Sakamoto, T. Inoue, and H. Sumiya, Ultrahard polycrystalline diamond from graphite, Nature (London) **421**, 599 (2003).
[2] V. N. Mochalin, O. Shenderova, D. Ho, and Y. Gogotsi, The properties and applications of nanodiamonds, Nat. Nanotechnol. **7**, 11 (2012).
[3] L. Wei, P. K. Kuo, R. L. Thomas, T. R. Anthony, and W. F. Banholzer, Thermal Conductivity of Isotopically Modified Single Crystal Diamond, Phys. Rev. Lett. **70**, 3764 (1993).
[4] H. Kanda, M. Akaishi, and S. Yamaoka, New catalysts for diamond growth under high pressure and high temperature, Appl. Phys. Lett. **65**, 784 (1994).
[5] Y. A. Mankelevich and P. W. May, New insights into the mechanism of CVD diamond growth: Single crystal diamond in MW PECVD reactors, Diam. Relat. Mater. **17**, 1021 (2008).
[6] Q. Huang, D. Yu, B. Xu, W. Hu, Y. Ma, Y. Wang, Z. Zhao, B. Wen, J. He, Z. Liu, and Y. Tian, Nanotwinned diamond with unprecedented hardness and stability, Nature (London) **510**, 250 (2014).
[7] P. Decarli and J. Jamieson, Formation of diamond by explosive shock, Science **133**, 1821 (1961).
[8] H. Tang, M. Wang, D. He, Q. Zou, Y. Ke, and Y. Zhao, Synthesis of nano-polycrystalline diamond in proximity to industrial conditions, Carbon **108**, 1 (2016).
[9] D. J. Erskine and W. J. Nellis, Shock-induced martensitic phase transformation of oriented graphite to diamond, Nature (London) **349**, 317 (1991).
[10] D. Kraus *et al.*, Nanosecond formation of diamond and lonsdaleite by shock compression of graphite, Nat. Commun. **7**, 10970 (2016).
[11] S. J. Turneaure, S. M. Sharma, T. J. Volz, J. M. Winey, and Y. M. Gupta, Transformation of shock-compressed graphite to hexagonal diamond in nanoseconds, Sci. Adv. **3**, eaao3561 (2017).
[12] S. Fahy, S. G. Louie, and M. L. Cohen, Pseudopotential total-energy study of the transition from rhombohedral graphite to diamond, Phys. Rev. B **34**, 1191 (1986).
[13] S. Scandolo, M. Bernasconi, G. L. Chiarotti, P. Focher, and E. Tosatti, Pressure-Induced Transformation Path of Graphite to Diamond, Phys. Rev. Lett. **74**, 4015 (1995).
[14] Y. Tateyama, T. Ogitsu, K. Kusakabe, and S. Tsuneyuki, Constant-pressure first-principles studies on the transition states of the graphite-diamond transformation, Phys. Rev. B **54**, 14994 (1996).
[15] F. Zipoli, M. Bernasconi, and R. Martoňák, Constant pressure reactive molecular dynamics simulations of phase transitions under pressure: The graphite to diamond conversion revisited, Eur. Phys. J. B **39**, 41 (2004).

[16] R. Z. Khaliullin, H. Eshet, T. D. Kühne, J. Behler, and M. Parrinello, Nucleation mechanism for the direct graphite-to-diamond phase transition, Nat. Mater. **10**, 693 (2011).
[17] V. D. Blank, B. A. Kulnitskiy, I. A. Perezhogin, E. V. Tyukalova, and V. N. Denisov, Graphite-to-diamond (13C) direct transition in a diamond anvil high-pressure cell, Int. J. Nanotechnology **13**, 604 (2016).
[18] Y. Gao, Y. Ma, Q. An, V. Levitas, Y. Zhang, B. Feng, J. Chaudhuri, and W. A. Goddard, Shear driven formation of nano-diamonds at sub-gigapascals and 300 K, Carbon **146**, 364 (2019).
[19] M. Álvarez-Murga, P. Bleuet, G. Garbarino, A. Salamat, M. Mezouar, and J. L. Hodeau, "Compressed Graphite" Formed During C60 to Diamond Transformation as Revealed by Scattering Computed Tomography Phys. Rev. Lett. **109**, 025502 (2012).
[20] V. D. Blank, B. A. Kulnitskiy, A. N. Kirichenko, N. R. Memetov, T. P. Dyachkova, and A. G. Tkachev, Features of structures obtained by graphene nanoplatelets treatment in a diamond anvil high-pressure cell, Fuller. Nanotub. Carbon Nanostructures **25**, 488 (2017).
[21] T. B. Shiell, D. G. McCulloch, J. E. Bradby, B. Haberl, R. Boehler, and D. R. McKenzie, Nanocrystalline hexagonal diamond formed from glassy carbon, Sci. Rep. **6**, 37232 (2016).
[22] S. Wong, T. B. Shiell, B. A. Cook, J. E. Bradby, D. R. McKenzie, and D. G. McCulloch, The shear-driven transformation mechanism from glassy carbon to hexagonal diamond, Carbon **142**, 475 (2019).
[23] W. Kohn and L. J. Sham, Self-consistent equations including exchange and correlation effects, Phys. Rev. **140**, A1133 (1965).
[24] C. J. Mundy, A. Curioni, N. Goldman, I.-F. Will Kuo, E. J. Reed, L. E. Fried, and M. Ianuzzi, Ultrafast transformation of graphite to diamond: An ab initio study of graphite under shock compression, J. Chem. Phys. **128**, 184701 (2008).
[25] G. Kresse and J. Furthmüller, Efficient iterative schemes for ab initio total-energy calculations using a plane-wave basis set, Phys. Rev. B **54**, 11169 (1996).
[26] G. Kresse and J. Furthmüller, Efficiency of ab-initio total energy calculations for metals and semiconductors using a plane-wave basis set, Comput. Mater. Sci. **6**, 15 (1996).
[27] L. Wen and H. Sun, Understanding shear-induced sp^2-to-sp^3 phase transitions in glassy carbon at low pressure using first-principles calculations, Phys. Rev. B **98**, 014103 (2018).
[28] See Supplemental Material at http://link.aps.org/supplemental/10.1103/PhysRevLett.124.065701 for calculation and experiment methods, SEM and TEM images of NG spheres, pressure dependence of the *G*-band frequencies and maximum shear stress as functions of the chamber pressure for two NG spheres, x-ray diffractions of the pristine NG and of the two NG spheres at 46 GPa, Raman spectra of pristine and the decompressed NG spheres, HRTEM image, and EELS of the released NG sample from a (quasi)hydrostatic pressure of 108 GPa, which includes Refs. [29–32].
[29] R. Debord, D. Leguillon, G. Syfosse, and M. Fischer, A finite element study of a high-pressure/high-temperature cell for simultaneous X-ray and ultrasonic measurement, High Press. Res. **23**, 451 (2003).
[30] B. Zhang and W. Guo, Cracking diamond anvil cells by compressed nanographite sheets near the contact edge, Appl. Phys. Lett. **87**, 051907 (2005).
[31] W. Guo, C. Z. Zhu, T. X. Yu, C. H. Woo, B. Zhang, and Y. T. Dai, Formation of sp^3 Bonding in Nanoindented Carbon Nanotubes and Graphite, Phys. Rev. Lett. **93**, 245502 (2004).
[32] http://www.matweb.com/.
[33] Y. Lin, L. Zhang, H. K. Mao, P. Chow, Y. Xiao, M. Baldini, J. Shu, and W. L. Mao, Amorphous Diamond: A High-Pressure Superhard Carbon Allotrope, Phys. Rev. Lett. **107**, 175504 (2011).
[34] M. Yao, J. Xiao, X. Fan, R. Liu, and B. Liu, Transparent, superhard amorphous carbon phase from compressing glassy carbon, Appl. Phys. Lett. **104**, 021916 (2014).
[35] M. Yao, X. Fan, W. Zhang, Y. Bao, R. Liu, B. Sundqvist, and B. Liu, Uniaxial-stress-driven transformation in cold compressed glassy carbon, Appl. Phys. Lett. **111**, 101901 (2017).
[36] Y. Akahama and H. Kawamura, Pressure calibration of diamond anvil Raman gauge to 310GPa, J. Appl. Phys. **100**, 043516 (2006).
[37] L. Dubrovinsky, N. Dubrovinskaia, V. B. Prakapenka, and A. M. Abakumov, Implementation of micro-ball nanodiamond anvils for high-pressure studies above 6 Mbar, Nat. Commun. **3**, 1163 (2012).
[38] N. Dubrovinskaia, L. Dubrovinsky, N. A. Solopova, A. Abakumov, S. Turner, M. Hanfland, E. Bykova, M. Bykov, C. Prescher, V. B. Prakapenka, S. Petitgirard, I. Chuvashova, B. Gasharova, Y.-L. Mathis, P. Ershov, I. Snigireva, and A. Snigirev, Terapascal static pressure generation with ultrahigh yield strength nanodiamond, Sci. Adv. **2**, e1600341 (2016).
[39] M. I. Eremets, I. A. Trojan, P. Gwaze, J. Huth, R. Boehler, and V. D. Blank, The strength of diamond, Appl. Phys. Lett. **87**, 141902 (2005).
[40] A. F. Goncharov, I. N. Makarenko, and S. M. Stishov, Graphite at pressure up to 55 GPa: optical properties and Raman scattering-amorphous carbon, Sov. Phys. JETP **69**, 380 (1989).
[41] Y. Wang, J. E. Panzik, B. Kiefer, and K. K. M. Lee, Crystal structure of graphite under room-temperature compression and decompression, Sci. Rep. **2**, 520 (2012).
[42] S. M. Clark, K.-J. Jeon, J.-Y. Chen, and C.-S. Yoo, Few-layer graphene under high pressure: Raman and X-ray diffraction studies, Solid State Commun. **154**, 15 (2013).
[43] J. Dong, X. Dai, L. Zhu, Y. Wang, H. Ma, M. Yao, G. Zou, R. Liu, and B. Liu, Transparent aerogel-like diamond nanofilms from glassy carbon by high pressure and high temperature, Diam. Relat. Mater. **96**, 90 (2019).
[44] T. B. Shiell, D. G. McCulloch, D. R. McKenzie, M. R. Field, B. Haberl, R. Boehler, B. A. Cook, C. de Tomas, I. Suarez-Martinez, N. A. Marks, and J. E. Bradby, Graphitization of Glassy Carbon after Compression at Room Temperature, Phys. Rev. Lett. **120**, 215701 (2018).
[45] J. R. Patterson, A. Kudryavtsev, and Y. K. Vohra, X-ray diffraction and nanoindentation studies of nanocrystalline graphite at high pressures, Appl. Phys. Lett. **81**, 2073 (2002).